BMC Pulmonary Medicine

RESEARCH

Open Access

Multiple Tumor-related autoantibodies test enhances CT-based deep learning performance in diagnosing lung cancer with diameters < 70 mm: a prospective study in China

Qingcheng Meng[1], Pengfei Ren[2], Lanwei Guo[3], Pengrui Gao[1], Tong Liu[1], Wenda Chen[1], Wentao Liu[1], Hui Peng[1], Mengjia Fang[1], Shuo Meng[4], Hong Ge[5*], Meng Li[6*] and Xuejun Chen[1*]

Abstract

Background Deep learning (DL) demonstrates high sensitivity but low specificity in lung cancer (LC) detection during CT screening, and the seven Tumor-associated antigens autoantibodies (7-TAAbs), known for its high specificity in LC, was employed to improve the DL's specificity for the efficiency of LC screening in China.

Purpose To develop and evaluate a risk model combining 7-TAAbs test and DL scores for diagnosing LC with pulmonary lesions < 70 mm.

Materials and methods Four hundreds and six patients with 406 lesions were enrolled and assigned into training set ($n = 313$) and test set ($n = 93$) randomly. The malignant lesions were defined as those lesions with high malignant risks by DL or those with positive expression of 7-TAAbs panel. Model performance was assessed using the area under the receiver operating characteristic curves (AUC).

Results In the training set, the AUCs for DL, 7-TAAbs, combined model (DL and 7-TAAbs) and combined model (DL or 7-TAAbs) were 0.771, 0.638, 0.606, 0.809 seperately. In the test set, the combined model (DL or 7-TAAbs) achieved achieved the highest sensitivity (82.6%), NPV (81.8%) and accuracy (79.6%) among four models, and the AUCs of DL model, 7-TAAbs model, combined model (DL and 7-TAAbs), and combined model (DL or 7-TAAbs) were 0.731, 0.679, 0.574, and 0.794, respectively.

Conclusion The 7-TAAbs test significantly enhances DL performance in predicting LC with pulmonary leisons < 70 mm in China.

*Correspondence:
Hong Ge
gehong666@126.com
Meng Li
lmcams@163.com
Xuejun Chen
zlyychenxuejun1943@zzu.edu.cn

Full list of author information is available at the end of the article

Key points

λ Deep learning exhibits high sensitivity but low specificity in LC diagnosis.

λ 7-TAAbs demonstrates high specificity but low sensitivity for early-stage LC, yet its application in China remains underexplored.

λ The complementary relationship between 7-TAAbs and DL may improve early LC diagnosis.

Keywords X-ray computed tomography, Tumor biomarkers, Deep learning, Neoplasm, pulmonary lesions

Introduction

Lung cancer (LC) is the leading cause of cancer-related deaths in China, accounting for 40.58% and 16.24% of cancer-related mortality in males and females, respectively [1]. Early detection and radical resection can significantly prolong the survival time of patients. Low-dose spiral computed tomography (LDCT) is highly sensitive for the early detection of small lung nodules, which is able to reduce LC mortality by 20% in screening within high-risk population [2]. However, the interpretation of large volumes of ultro-thin LDCT slices by radiologists is both labor-intensive and time-consuming, inevitably increasing the risk of missed diagnosis and misdiagnosis [3]. Therefore, it is necessary to provide reliable computer aided detection (CAD) as a decision support tool for radiologists to improve diagnostic efficiency and reduce the burden of manual screening. Among CAD techniques, deep learning (DL) has demonstrated remarkable performance in lung nodules detection using CT images [4–10]. Ardila D, et al. [11] proposed a deep learning algorithm utilizing a patient's current and previous computed tomography volumes to predict the risk of lung cancer in 6,716 National Lung Cancer Screening Trial cases and achieved 94.4% area under the curve.The study of Baldwin DR, et al. [12] showed that the convolutional neural network (LCP-CNN) achieved the area under the receiver operating characteristic curves (AUC) of 89.6% and false negative rate of 0.4% for incidentally detected t5-15 mm pulmonary nodules. In contrast, our previous study showed that the deep learning based on multi-stage three-dimensional deep convolutional neural network (3D-DCNN) algorithms only achieved a modest AUC of 0.606 (0.366–0.845) in risk stratification management of pulmonary ground-glass nodules [13]. Therefore, the current DL models still face critical barriers obstructing the early diagnosis of LC, such as high false positive rate, high cost, more image data, and low calculation efficiency.

Combined with non-invasive biomarkers, CT may contribute to earlier detection of lung cancer and shorter follow-up time, which has the potential to reduce false positive rate and false negative rate in screening [14–16]. Tumor-associated antigens (TAAs) are abnormal proteins expressed in tumor cells, which may elicit the autoimmune response and result in the production of circulating autoantibodies against TAAs (TAAbs). These TAAbs exhibit high specificity in the clinical diagnosis of lung cancer and can be used as potential noninvasive biomarkers for the early detection and monitoring of LC [17–19]. Previous studies have shown that a multi-TAAb pannel test significantly improves sensitivity across all LC stages compared to single-TAAb assays, though overall sensitivity remains suboptimal [20]. We presume that the combination of imaging-based deep learning with molecular biomarkers might be useful in the characterization of indeterminate pulmonary nodules. To this end, we designed a diagnosis model by combining a deep learning-based three-dimensional deep convolutional neural network (3D-DCNN) with 7-TAAbs to discriminate malignant from benign pulmonary lesions, aiming to improve early LC detection rate.

Materials and methods

Patient characteristics

Four hundards and ninety-nine patients with high-risk pulmonary lesions were enrolled in this prospective study and were underwent chest CT scan and the 7-TAAbs test in the Affiliated Cancer Hospital of Zhengzhou University & Henan Cancer Hospita from April 2021 to January 2024. **Inclusion criteria**: (1) Chest CT revealed indeterminate pulmonary lesions with diameters < 70 mm; (2) No history of tuberculosis or pneumonia recently; (3) No history of lung cancer or thoracic malignancies known currently. **Exclusion criteria**: (1) Patients with TNM stages ≥ IIIB defined by PET-CT; (2) Patients lost to three-year follow-up period; (3) Patients suffering from immunodeficiencies or immune hyperfunction; (4) Patients with lung or other organ infections. Two hundreds and twelve observations underwent surgical resection after 10–15 days of chest CT scan, and 194 observations were diagnosed as perifissural nodule (PFN) [21] or pneumonia after 36–60 months follow-up. Regarding the issue of multiple lesions in the same patient, in order to avoid the heterogeneity of the expression of the 7-TAAbs in different lesions of the same patient, this study only selected the largest lesion as the research object. Eventually 406 patients with 406 observations were enrolled in this study, which was grouped as the training set ($n = 313$) and the test set ($n = 93$). The selection process of subjects in this study was depicted in Fig. 1.

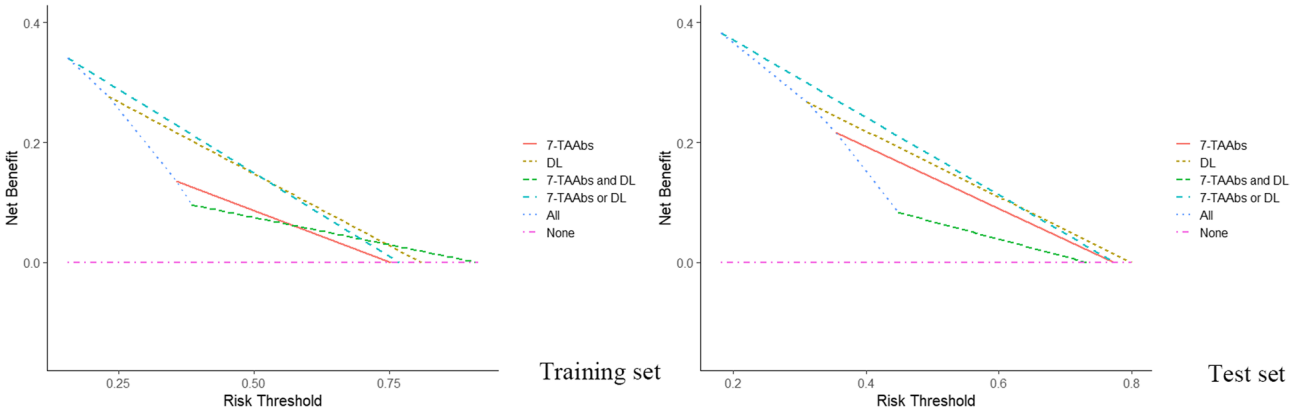

Fig. 1 Flowchart of the patient selection procedure. Abbreviations: CT: computer tomography; 7-TAAbs: seven autoantibodies against tumor-associated antigens

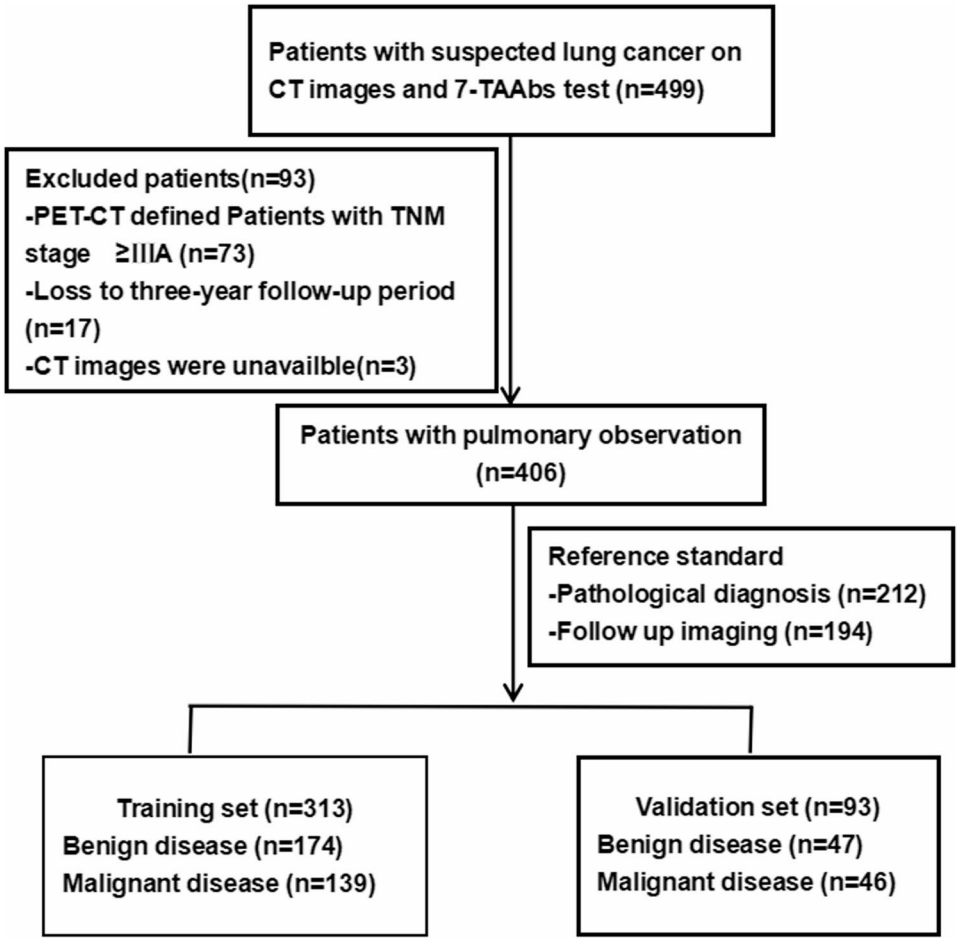

Fig. 2 The flowchart of ELISA in this study

Autoantibody assay

Blood samples were collected from all patients within two weeks prior to surgery or before follow-up chest CT examinations The serum was separated and stored immediately at −80 ℃ for later use. Concentration of seven autoantibodies against p53, PGP9.5, SOX2, GAGE7, GBU4-5, MAGE A1 and CAGE were measured by indirect enzyme-linked immunosorbent assay with a commercially ELISA kit (Cancer Probe Biological Technology Co. Ltd., Hangzhou, China) [22], following the according to the manufacture's protocol (Fig. 2). In brief, serum samples and detection kit components were equilibrated

to room temperature previously. Seven antigens used to detect 7-AAbs in the serum samples were coated onto the 96 wells microplate by the manufacturers, and the microplates were washed one time with 280 ul of PBS before diluted sera were added into the wells. Then, serum samples were diluted as 1: 109 with serum dilutions, 50 ul diluted sera, standards and controls were added into the antigen-coated wells and incubated for 1 h at room temperature, then washed three times with PBST, 280 ul for each well. Next 50ul of diluted secondary antibodies, HRP conjugated goat anti-human IgG, were added into the wells and incubated for 30 min at room temperature, and then the microplates were washed three times with PBST. Thereafter, 100 ul of substrate was added, followed by plate incubation for 15 min at room temperature. After that, 50 ul of stop solution was added to each well and mixed thoroughly. The optical density was measured at 450 nm within 30 min using a spectrophotometer.

CT image acquisition

All enrolled patients underwent LDCT or standard-dose CT using multidetector CT scaners (LightSpeed-16, GE; iCT-256, Siemens). The protocol parameters were 120 KVp and 30 mAs for LDCT, or 120 KVp and 200 mAs for routine CT, 512 × 512 matrix, field of view 400 mm × 4 00–500 mm × 500 mm, collimation 128 × 0.625 mm or 16 × 1.25 mm, rotation 0.5 s, pitch 0.8 or 1.02, 1.25 mm section width with a 1.25 mm reconstruction interval, and duration of scan 3–10 s. Unenhanced spiral acquisitions were performed during a breath-hold, covering from the thoracic inlet to lung bases. Images were reconstructed in axial planes for analysis.

Commercial Deep learning framework based on multi-stage 3D DCNN algorithms and its standard of risk stratification of pumlmonary lesions

The technique of DL approach supported by Beijing medical technology co. LTD was authorized used and the GUI mechanical registration approval number was 20,182,700,040. The framework of commercial DL was based on 3D-DCNN algorithms [23]. The DL algorithm of the lung nodule diagnosis model comprises two stages. First, the Faster R-CNN to propose a DCNN model for **detecting nodule candidates** from the CT images, as shown in Fig. 3. In the following section, we describe the details of the architecture of the proposed candidate detection network. The network is composed of two modules: a region proposal network (RPN) that is aimed at identifying a potential region-of-interest (ROI), and an ROI classifier that recognizes whether the ROIs are nodules or not. To reduce the computation cost of training the model, the two DCNN modules were made to share the same feature extraction layers.

Second stage was used for reducing the false positive rate as following. Using the ROIs extracted by RPN, a DCNN was developed to determine if an ROI was a nodule or not. An ROI Pooling layer was firstly exploited to map each ROI to a small feature map with a fixed spatial extent of 7×7. After the ROI pooling layer, a fully connected network, which is composed of two 4096-way fully connected 4 layers, then mapped the fixed-size feature map onto a feature vector. A regressor and a classifier based on the feature vector (i.e. BBox Reg and BBox Cls) were then used to respectively regress the bounding boxes of the candidates and predict candidate confidence scores. In the training process, the RPN and ROI classifier were merged into a single network, and the loss functions for the images were defined, specific details are available in Ren et al. [24]. Subsequently, with the extracted nodule candidates, a 3D DCNN was utilized for nodule malignancy prediction, which captures the entire range of contexts of the candidates and generates more discriminative features than 2D DCNNs. This network contains six 3D convolutional layers, which are followed by the rectified linear unit (ReLU) activation layers, three 3D max-pooling layers, three fully connected layers, and a final 2-way softmax activation layer to classify the candidates as nodules or non-nodules. Furthermore, the dropout layers were added after the max-pooling and fully-connected layers to avoid overfitting. Each CT scan

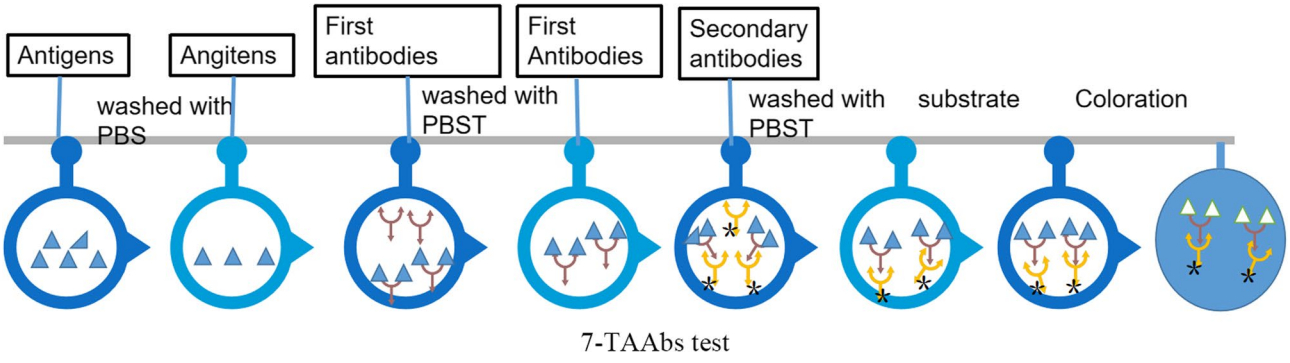

Fig. 3 The frame structure of deep learning based on multi-stage three-dimensional deep convolutional neural networ (3D-DCNN)

was first normalized with a mean of −600 and a standard deviation of −300, and the center of the candidate was used as the centroid, and subsequently a 40 × 40 × 24 patch was used for each candidate. To balance the number of positive and negative patches in the training set, the positive patches were duplicated for 8 times. The degrees of malignancy of the detected nodules by the DL approach were classified as low, medium and high risk for malignant pulmonary lesions.

Imaging, serum taabs, and histopathologic evaluation

The results for the number, sizes, types, distribution of nodules, and CT characteristics were confirmed by the consensus of three thoracic radiologists with 7, 10, and 15 years of experience. The PFNs were diagnosed by the consensus of three thoracic radiologists after 36–60 months CT scan follow-up, and the malignant lesions were defined as those lesions with high malignant risks by DL or those with positive expression of TAAbs including one or more positive result of the 7-TAAbs panel. The eighth edition of lung cancer stage classification was utilized to determine the histopathology and stage of the lung cancer [25].

Table 1 Clinical characteristics of patients between training set and test set (means ± standard deviations (SD); n (%))

Characteristics	Training set (*n* = 313)	Test set (*n* = 93)	*P*
Gender			
Male	184 (58.8)	56 (60.2)	0.806
Female	129(41.2)	37 (39.8)	
Age (y)	56.21 ± 11.20	57.56 ± 11.19	0.310
Chronic obstructive pulmonary disease			0.601
Yes	40 (12.8)	10 (10.8)	
No	273(87.2)	83(89.2)	
History of smoking			
Yes	92(29.4)	20(21.5)	0.135
No	221(70.6)	73(78.5)	
History of cancer			
Yes	40(12.8)	8(8.6)	0.273
No	273(87.2)	85(91.4)	
Pneumonia			
Yes	43(13.7)	12(12.9)	0.836
No	270(86.3)	81(87.1)	
Size of lesions			0.998
<30 mm	231 (73.8)	69(74.2)	
≥ 30 mm, <50 mm	58 (18.5)	17(18.3)	
≥ 50 mm, <70 mm	24 (7.7)	7(7.5)	
Type of lesions			0.006
GGN	59 (18.8)	6(6.4)	
PSN	15(4.8)	2 (2.2)	
SN	239(76.4)	85 (91.4)	
Lung diseases spectrum			0.478
Benign diseases	174 (55.6)	47(50.5)	
Adenocarcinoma	104 (33.2)	33 (35.5)	
SCC	20 (6.4)	10 (10.8)	
SCLC	11(3.5)	3 (3.2)	
Adenosquamous carcinoma	4 (1.3)	0 (0.0)	
Expression of 7-TAAbs			0.177
Positive	73 (23.3)	27(29.0)	
Negative	240 (76.7)	66 (71.0)	

Abbreviations: *GGNs* ground-glass nodules, *PSN* part-solid nodules, *SN* solid nodules, *7-TAAbs* seven tumor-associated antigen autoantibodies, *LC* lung cancer, *SCC* Squamous cell carcinoma, *SCLC* small cell lung cancer, *COPD* chronic obstructive pulmonary disease

Statistical analysis

All statistical analysis were performed using tSPSS version 24.0 (IBM Corp.) and R software (for decision curves analysis). All continuous variables are presented by means ± standard deviations (SD) and compared by t test. The counting data were described with frequency or percentage and compared by Chi-square test. We evaluated four distinct risk stratification model (Table 3): 7-TAAbs model, DL model, integrated combined model (7-TAAbs and DL), integrated combined model (7-TAAbs or DL). The diagnostic performance of four risk stratification models were evaluated using standard metrics, including sensitivity, specificity, accuracy, positive predictive value (PPV), and negative predictive value (NPV). In the discrimination of the malignant nodules, the performance was assessed via a receiver operating characteristics curve (ROC) analysis for all the risk models. Additionally, decision curve analysis (DCA) was performed using R to evaluate clinical utility.The tests were two-sided, and the statistical significance was set to $P < 0.05$.

Results

Patient and lesion characteristics

As shown in Table 1, the training set comprised 139 malignant observations (104 adenocarcinomas, 20 squamous cell carcinomas (SCCs), 11 small-cell lung cancers (SCLCs), and 4 adenosquamous carcinomas) and 174 benign lesions, while the test set inclued 46 malignant observations (33 adenocarcinomas, 10 SCCs, 3 SCLCs) and 47 benign lesions. Based on nodule density, the cohort was further divided into 65 pure ground-glass nodules, 17 part-solid nodules and 324 solid nodules between the training set and test set ($P < 0.05$). Furthermore, the sizes of 300 lesions were less than 30 mm, 75 lesions were ≥ 30 mm but < 50 mm, 31 lesions were ≥ 50 mm but < 70 mm. No significant differences ($P > 0.05$) was observed between the training and test sets in terms of the sex, age, chronic obstructive pulmonary disease, history of smoking, history of cancer, pneumonia, lung diseases spectrum, size of nodules, and the positive rate of 7-TAAbs.

The positive expression of 7-TAAbs and its risk factors analysis of pulmonary lesions

In this study, a total of 100 observations tested positive for 7-TAAbs, including 76 malignant lesions and 24 benign lesions. The 7-TAAbs assay demonstrated moderate performance with a sensitivity of 41.1% and specificity of 89.1% for LC diagnosis. In order to assess risk factors associated with pulmonary lesions, we performed predictors variables analysis including age, gender, chronic obstructive pulmonary disease, history of smoking, history of cancer, size of lesions, type of nodules, location of lesions, expression of 7-TAAbs and CT images (including lobation, vascular convergence sign, pleural indentation, bronchial truncation sign, spiculation sign, bronchogram, atelectasis and vacuole sign). The analysis revealed that only the expression of 7-TAAbs and the age were statistically significant predictors of LC (both $P < 0.05$), shown in Table 2.

Performance metrics of 7-TAAbs model, DL model, and the integrated conbined model ("7-TAAbs and DL", "7-TAAbs and DL") in risk stratification for incidental pulmonary lesions

In this study, 24 observations with 7-TAAbs positivity were obtained. However, comprehensive CT evaluation and longitudinal follow-up (36–60 months) confirmed these cases as pulmonary focal nodules (PFNs), irrespective of potential long-term malignant transformation (Table 1; Fig. 4). In the training set, the DL approach achieved a sensitivity of 66.9%, specificity of 87.9%, PPV of 81.6%, NPV of 76.9%, and accuracy of 78.6%. On the other hand, the 7-TAAbs approach yielded higher specificity with 90.2%, but markably lower 37.4% sensitivity and 66.8% accuracy. Compared with the DL or 7-TAAbs approach, the combined model (DL and 7-TAAbs) yielded exceptional specificity (98.3%), and PPV (91.4%) but sensitivity (23.0%) and accuracy (64.9%). The combined model (DL or 7-TAAbs) approach yielded improved sensitivity (81.3%) and NPV (84.5%) but lower specificity (81.6%) and PPV (77.9%). The AUCs of DL model, 7-TAAbs model, combined model (DL and 7-TAAbs), and combined model (DL or 7-TAAbs) were 0.771 (95% CI: 0.716–0.826), 0.638 (95% CI: 0.575–0.701), 0.606 (95% CI: 0.542–0.671) and 0.809 (95% CI: 0.758–0.859), respectively (shown in Table 3).

In the test set, the combined model (DL or 7-TAAbs) achieved the optimal sensitivity (82.6%), NPV (81.8%) and accuracy (79.6%) among all evaluated approaches. However, the combined model (DL and 7-TAAbs) yielded a superior specificity (91.5%) than the single DL or 7-TAAbs approach. The AUCs of DL, 7-TAAbs, combined model (DL and 7-TAAbs), and combined model (DL or 7-TAAbs) were 0.731 (95% CI: 0.628–0.833), 0.679 (95% CI: 0.571–0.787), 0.574 (95% CI: 0.459–0.688), and 0.794 (95% CI: 0.701–0.887),respectively (shown in Table 3). The combined model (DL or 7-TAAbs) emerged as the most clinically applicable model, demonstrating balanced diagnostic performance for lung cancer detection (Figs. 5 and 6). This combined approach effectively leveraged the complementary strengths of both modalities, optimizing sensitivity while maintaining reasonable specificity.

Discussion

This study enrolled 406 patients with incidental pulmonary lesions to evaluate the diagnostic performance of 7-TAAbs, DL and combined models for LC detection. The results showed that the combined model (DL or 7-TAAbs) outperformed either approach alone or other combination models in the risk stratification management of pulmonary lesions, which achieved the highest sensitivity, NPV, accuracy and AUC in both training set and test set.

Among various biomarkers for LC, TAAbs have demonstraed clinical applicability. In a multicenter study performed in a Chinese population, the 7-TAAbs panel exhibited a sensitivity of 61% and a specificity of 90%. For early-stage NSCLC, its sensitivity was 62% (stage I) and 59% (stage II), while for limited stage small cell LC it achieved 59% sensitivity [22]. In our study, 100 observations have the positive of 7-TAAbs was positive in 100 cases (77 malignant, 23 benign), demonstrating 41.1% sensitivity and 89.1% specificity for LC diagnosis This relatively lower sensitivity compared to previous study may reflect differences in our inclusion criteria. A Early CDT-Lung test using a 7-TAAbs panel showed a 35.0% sensitivity and a 91.0% specificity [26], and Chen P et al. [27] aiso reported that 7-TAAbs alone lack sufficient diagnostic efficiency for primary NSCLC screening. He YT et al. [28] reported that age, smoking, SHS, dietary factors, occupational exposures, history of disease and family history of cancer may affect the incidence of pulmonary nodules, but our risk variables analysis idenfied only 7-TAAbs expression and age as significant risk factors for pulmonary malignancy, all of which might due to the relatively small sample size and selection bias.

These results suggest that while 7-TAAbs may not be ideal for primary screening, they could serve as a valuable biomarker for risk stratification of pulmonary lesions when combined with other diagnostic approaches.

The current era of artificial intelligence has facilitated significant progress in the field of radiology due to the accumulation of detailed imaging data. In our study, we employed a state-of-the-art multiple 3D-DCNN algorithm, based on the Faster R-CNN framework, which demonstrates robust performance in the characterization and discrimination of lung nodules [24]. However, this algorithm still faces challenges in addressing high

Table 2 Risk variables analysis of pulmonary malignant lesions

Characteristics	Total ($n=406$)	Pulmonary malignant lesions ($n=185$)	Pulmonary benign lesions($n=221$)	*P* value
Age (y)	63(52,74)	61(52,70)	53(42,64)	0.000
Gender				0.058
Male	240	100	140	
Female	166	85	81	
Chronic obstructive pulmonary disease				0.261
Yes	50	19	31	
No	356	166	190	
History of smoking				0.566
Yes	115	55	60	
No	291	130	161	
History of cancer				0.564
Yes	48	19	29	
No	358	166	192	
Size of lesions				0.912
< 30 mm	300	137	163	
≥ 30 mm, < 50 mm	75	34	41	
≥ 50 mm, < 70 mm	31	14	17	
Type of nodules				0.485
GGN	65	29	36	
PSN	17	7	10	
SN	324	149	175	
Expression of 7-TAAbs				0.000
Positive	100	77	23	
Negative	306	108	198	
Location				0.586
RUL	106	47	59	
RML	52	28	24	
RLL	95	45	50	
LUL	78	31	47	
LLL	75	34	41	
Lobation				0.878
Yes	176	80	96	
No	230	105	125	
Vascular convergence sign				0.984
Yes	66	30	36	
No	340	155	185	
Pleural indentation				0.572
Yes	57	24	33	
No	349	161	188	
Bronchial truncation sign				0.126
Yes	31	10	21	
No	375	175	200	
Spiculation sign				0.940
Yes	40	18	22	
No	366	167	199	
Bronchogram				0.544
Yes	13	7	6	
No	393	178	215	
Atelectasis				0.653
Yes	38	16	22	
No	368	169	199	

Table 2 (continued)

Characteristics	Total ($n=406$)	Pulmonary malignant lesions ($n=185$)	Pulmonary benign lesions($n=221$)	*P* value
Vacuole sign				0.514
Yes	23	12	11	
No	383	173	210	

Abbreviations: *GGNs* ground-glass nodules, *PSN* part-solid nodules, *SN* solid nodules, *7-TAAbs* seven tumor-associated autoantibodies, *COPD* chronic obstructive pulmonary disease, *RUL* right uper lobe, *RML* right middle lobe, *RLL* right low lobe, *LUL* left upper lobe, *LLL* left low lobe

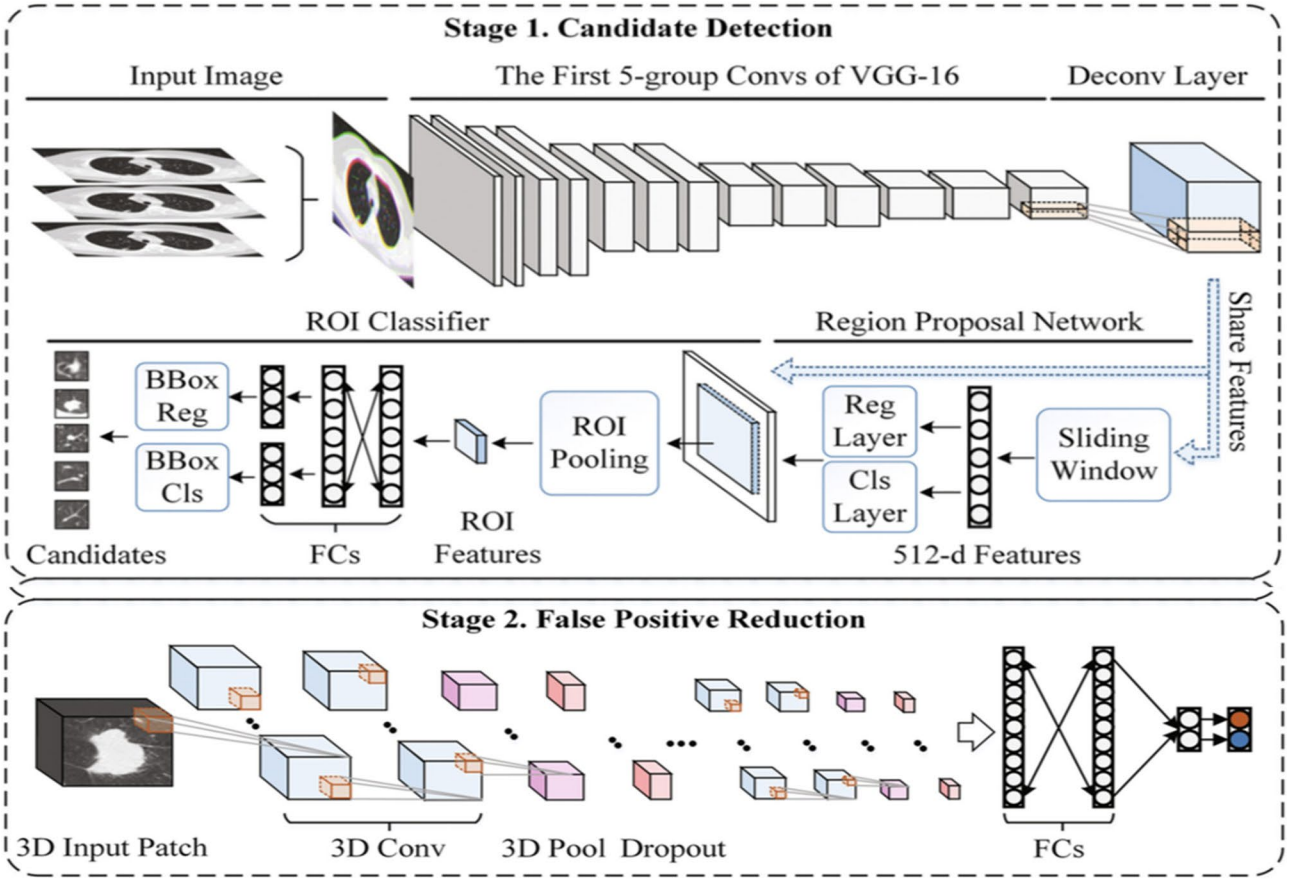

Fig. 4 On the chest CT images of a 58-year-old man, a triangle SN located on the horizontal fissure was low defined as low risk of malignant pulmonary disease by DL but with positive expression of 7-TAAbs, which was diagnosed as perifissural nodule by the consensus of the three thoracic radiologists due to its stable of size after more than two years follow-up (axial: 4a, coronal: 4b, sagittal: 4c)

false positive rate [29]. To address this, we implemented a modified R-CNN archhitecture to enhance its discriminative capability between benign and malignant lesions, and our DL model achieved a sensitivity of 66.9%, a specificity of 87.9% and an AUC of 0.771. Although our DL approach achieved a lower AUC than other studies, such as the one conducted by *Ardila D et al.* [11]. this difference may be attributable to differences in the study population. Notably, our combined model of DL and 7-TAAbs achieved superior performance, with 81.3% sensitivity, 84.5% NPV, 81.5% accuracy, and an AUC of 0.809 in the training set. These results were further validated in the test set, which suggests that this combination model may be the most effective approach for risk stratification of incidental pulmonary lesions in actual clinical scenarios.

There are several limitations in our study. First, the current TAAbs panel requires further optimization to improve its sensitivity for malignant lesions detection. Second, there were no enough controls in this study Previous studies have reported that circulating TAAbs could also be detected in other lung diseases such as interstitial lung disease, chronic obstructive pulmonary disease, and asthma [30, 31], therefore the inclusion criteria should be limited to specific patients to reduce the false positive rate of 7-TAAbs. Third, due to the phenomenon of the same disease may yield different CT images, while

Table 3 Diagnostic value for malignant pulmonary nodules with DL, 7-TAAbs, combined model ('DL and 7-TAAbs','DL or 7-TAAbs')

	Training set (*n*=313)				Test set (*n*=93)			
	DL	7-TAAbs	DL and 7-TAAbs	DL or 7-TAAbs	DL	7-TAAbs	DL and 7-TAAbs	DL or 7-TAAbs
TP	93	52	32	113	28	24	11	38
FP	21	17	3	32	7	7	4	11
FN	46	87	107	26	18	22	35	8
TN	153	157	171	142	40	40	43	36
Sensitivity, % (95% CI)	0.669 (0.587,0.742)	0.374 (0.298,0.457)	0.230 (0.168,0.307)	0.813 (0.740,0.869)	0.609 (0.465,0.736)	0.522 (0.381,0.659)	0.239 (0.139,0.379)	0.826 (0.693,0.909)
Specificity, % (95% CI)	0.879 (0.823,0.920)	0.902 (0.849,0.938）	0.983 (0.951,0.994)	0.816 (0.752,0.867)	0.851 (0.723,0.926)	0.851 (0.723,0.926)	0.915 (0.801,0.966)	0.766 (0.628,0.864)
PPV, % (95% CI)	0.816 (0.735,0.876)	0.754 (0.640,0.840)	0.914 (0.776,0.970）	0.779 (0.705,0.839)	0.8 (0.641,0.900)	0.774 (0.602,0.886)	0.733 (0.481,0.891)	0.776 (0.641,0.870)
NPV, % (95% CI)	0.769 (0.706,0.822)	0.643 (0.582,0.701)	0.615 (0.557,0.670)	0.845 (0.783,0.592)	0.690 (0.562,0.794)	0.645 (0.521,0.760)	0.551 (0.441,0.657)	0.818 (0.680,0.9050
Accuracy, % (95% CI)	0.786 (0.737,0.828)	0.668 (0.614,0.718)	0.649 (0.594,0.699)	0.815 (0.768,0.854)	0.688 (0.588,0.773)	0.688 (0.588,0.773)	0.581 (0.479,0.676)	0.796 (0.703,0.865)
AUC	0.771 (0.716,0.826)	0.638 (0.575, 0.701)	0.606 (0.542,0.671)	0.809 (0.758,0.859)	0.731 (0.628,0.833)	0.679 (0.571,0.787)	0.574 (0.459,0.688)	0.794 (0.701,0.887)

Abbreviations: *FN* false-negative, *FP* false-positive, *TN* true-negative, *TP* true-positive, *PPV* positive predictive value, *NPV* negative predictive value, *+LR* positive likelihood ratio, 95% *CI* confidence interval, *AUC* area under receiver operating characteristic curves

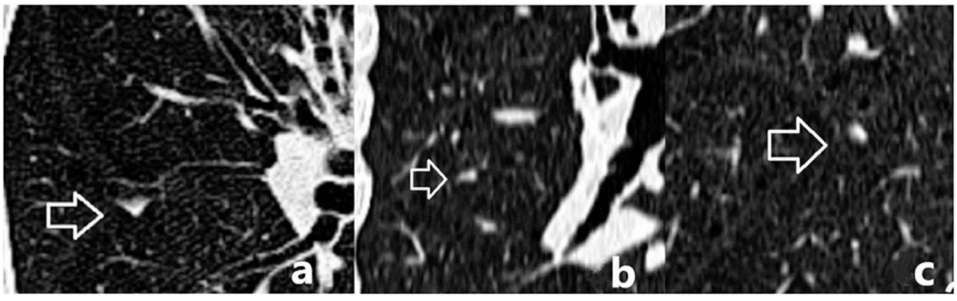

Fig. 5 Comparison of the AUCs of deep learning, 7-TAAbs, DL and 7-TAAbs in the training set and validation set. In the training set, the AUCs of DL, 7-TAAbs, DL and 7-TAAbs, and DL or 7-TAAbs were 0.771 (95% CI: 0.716–0.826), 0.638 (95% CI: 0.575–0.701), 0.606 (95% CI: 0.542–0.671) and 0.809 (95% CI: 0.758–0.859), respectively. In the test set, the AUCs of DL, 7-TAAbs, DL and 7-TAAbs, and DL or 7-TAAbs were 0.731 (95% CI: 0.628–0.833), 0.679 (95% CI: 0.571–0.787), 0.574 (95% CI: 0.459–0.688), and 0.794 (95% CI: 0.701–0.887) respectively. AUC = area under receiver operating characteristic curve, DL = deep learning, 7-TAAbs = seven autoantibodies against tumor-associated antigens

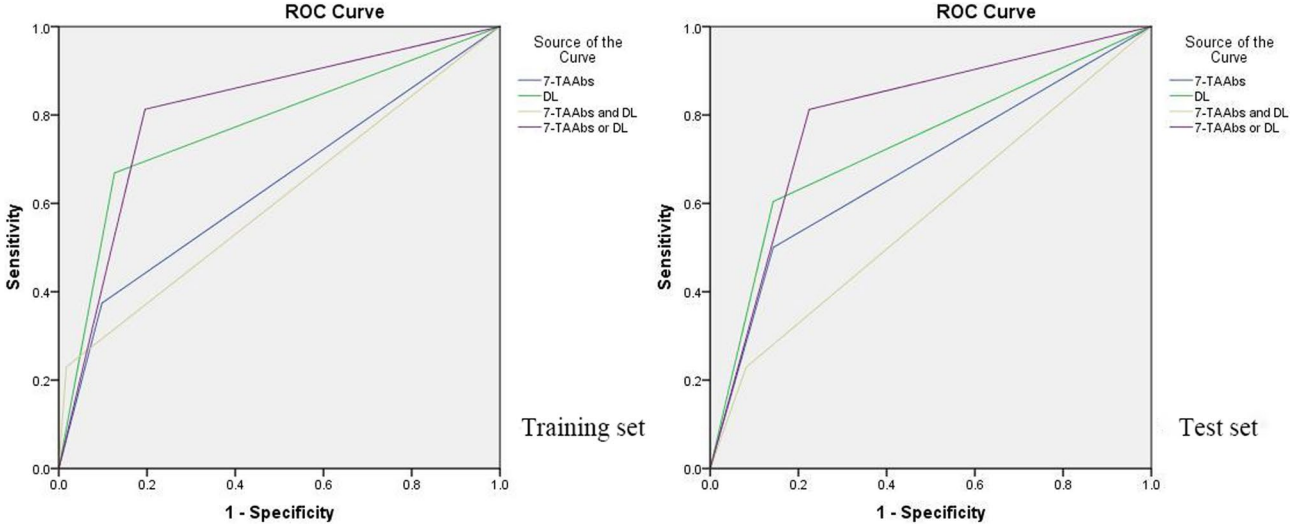

Fig. 6 Decision analysis curve of risk prediction model for lung cancer in training set and test set

identical CT images can be yield from different disease in clinical, so it is necessary to further develop deep learning techniques based on CT images and epidemiological features to improve the ability of artificial intelligence to distinguish benign and malignant nodules in clinical practice. Fourth, Regarding the issue of multiple lesions in the same patient in this study, only one largest lesion was selected as the research object, which might lead to selection bias.

In conclusion, our single-center cohort study identified 7-TAAbs expression and age as the only significant risk factors for pulmonary malignant lesions, whiles other variables (including chronic obstructive pulmonary disease, history of smoking, history of cancer, size of lesions, type of nodules, location of lesions and CT signs) showed no significant association. The multi-stage 3D DCNN deep learning model, while combined with 7-TAAbs analysis, demonstrated optimal diagnostic performance in the risk stratification for incidental pulmonary lesions. therefore, the diagnostic accuracy of incidental pulmonary lesions can be effectively improved in China. Further validation through large-scale, a multi-centre clinical trial is warranted to confirm the generalizability and clinical utility of these findings.

Abbreviations

DL	deep learning
LC	Lung cancer
LDCT	Low-dose spiral computed tomography
CAD	computer aided detection
TAAbs	tumor-related antigen autoantibodies
3D-DCNN	three-dimensional deep convolutional neural network
AUC	area under the receiver operating characteristic curves
PPV	positive predictive value
NPV	negative predictive value
95% CI	95% confidence interval

Acknowledgements
We would like to thank Editage (www.editage.cn) for the English language editing and Jia Ding et al. for DL technique permission.

Authors' contributions
Dr Qingcheng Meng had full access to all the data in the study and takes responsibility for the integrity of the data and the accuracy of the data analysis. Concept and design: All authors. Acquisition, analysis, or interpretation of data: All authors. Drafting of the manuscript: Qingcheng Meng. Critical revision of the manuscript for important intellectual content: Qingcheng Meng, Lanwei Guo, Tong Liu, Hui Peng. Statistical analysis: Lanwei Guo, Pengrui Gao. Administrative, technical, or material support: Wentao Liu. Supervision: Hong Ge, Meng Li, Xuejun Chen.

Funding
the design of the study and the collection, analysis, and interpretation of data were supported by the funds of the key project of medical science and technology of Henan province in China (Award number: SBGJ202102057) and the science and technology project of Henan province in China (Award number: 212102310744).

Data availability
The data sets are available from the corresponding author upon reasonable request.

Declarations

Ethics approval and consent to participate
This study was approved by the Affiliated Cancer Hospital of Zhengzhou University & Henan Cancer Hospital Medical Ethics Committee (2021-KY-0022) and complied with its ethical standards. Written informed consent was achieved by the patients.

Consent for publication
Not applicable.

Competing interests
The authors declare no competing interests.

Author details
[1]Department of Radiology, The Affiliated Cancer Hospital of Zhengzhou University & Henan Cancer Hospital, Zhengzhou, China
[2]Department of Molecular Pathology, The Affiliated Cancer Hospital of Zhengzhou University & Henan Cancer Hospital, Zhengzhou, China
[3]Department of Clinical Research Management, The Affiliated Cancer Hospital of Zhengzhou University & Henan Cancer Hospital, Zhengzhou 450008, China
[4]Department of Mechanical and Electrical Engineering, Beijing University of Chemical Technology, Beijing, China
[5]Department of Radiotherapy, The Affiliated Cancer Hospital of Zhengzhou University & Henan Cancer Hospital, Zhengzhou, China
[6]Department of Radiology, National Clinical Research Center for Cancer/Cancer Hospital, National Cancer Center, Chinese Academy of Medical Sciences, Peking Union Medical College, Beijing, China

Received: 22 July 2024 / Accepted: 23 June 2025
Published online: 29 July 2025

References

1. Zheng RS, Zhang SW, Zeng HM, Wang SM, Sun KX, Chen R, Li L, Wei WQ, He J. Cancer incidence and mortality in china, 2016. J Natl Cancer Cent. 2022;2(1):1–9. https://doi.org/10.1016/j.jncc.202.02.002..DOI:.
2. The National Lung Screening Trial Research Team. Reduced lung-cancer mortality with low-dose computed tomographic screening. N Eng J Med. 2011;365(5):395–409. https://doi.org/10.1056/NEJMoa1102873.
3. Li F, Sone S, Abe H, MacMahon H, Armato SG III. Doi.Lung cancers missed at low-dose helical CT screening in a general population: comparison of clinical, histopathologic, and imaging findings. Radiology. 2002;225(3):673–83. https://doi.org/10.1148/radiol.2253011375.
4. Wang Q, Shen F, Shen L, Huang J, Sheng W. Lung nodule detection in CT images using a Raw patch-based convolutional neural network. J Digit Imaging. 2019;32(6):971–9. https://doi.org/10.1007/s10278-019-00221-3.
5. Pehrson LM, Nielsen MB, Ammitzbøl Lauridsen C. Automatic pulmonary nodule detection applying deep learning or machine learning algorithms to the LIDC-IDRI database: A systematic review 2019;9(1):29. https://doi.org/10.3390/diagnostics9010029
6. Ye W, Gu W, Guo X, et al. Detection of pulmonary ground-glass opacity based on deep learning computer artificial intelligence. Biomed Eng Online. 2019;18(1):6. https://doi.org/10.1186/s12938-019-0627-4.
7. Li L, Liu Z, Huang H, Lin M, Luo D. Evaluating the performance of a deep learning-based computer-aided diagnosis (DL-CAD) system for detecting and characterizing lung nodules: comparison with the performance of double reading by radiologists. Thorac Cancer. 2019;10(2):183–92. https://doi.org/10.1111/1759-7714.12931.
8. Eun H, Kim D, Jung C, Kim C. Single-view 2D CNNs with fully automatic non-nodule categorization for false positive reduction in pulmonary nodule detection. Comput Methods Programs Biomed. 2018;165:215–24. https://doi.org/10.1016/j.cmpb.2018.08.012.
9. Shaffie A, Soliman A, Fraiwan L, et al. A generalized deep Learning-Based diagnostic system for early diagnosis of various types of pulmonary nodules. Technol Cancer Res Treat. 2018;17:1533033818798800. https://doi.org/10.1177/1533033818798800.

10. Xie Y, Xia Y, Zhang J, et al. Knowledge-based collaborative deep learning for Benign-Malignant lung nodule classification on chest CT. IEEE Trans Med Imaging. 2019;38(4):991–1004. https://doi.org/10.1109/TMI.2018.2876510.
11. Ardila D, Kiraly AP, Bharadwaj S, et al. End-to-end lung cancer screening with three-dimensional deep learning on low-dose chest computed tomography. Nat Med. 2019;25(6):954–61. https://doi.org/10.1038/s41591-019-0447-x.
12. Baldwin DR, Gustafson J, Pickup L, et al. External validation of a convolutional neural network artificial intelligence tool to predict malignancy in pulmonary nodules. Thorax. 2020;75(4):306–12. https://doi.org/10.1136/thoraxjnl-2019-214104.
13. Meng Q, Li B, Gao P, et al. Development and validation of a risk stratification model of pulmonary Ground-Glass nodules based on complementary Lung-RADS 1.1 and deep learning scores. Front Public Health. 2022;10:891306. https://doi.org/10.3389/fpubh.2022.891306.
14. Massion PP, Healey GF, Peek LJ, et al. Autoantibody signature enhances the positive predictive power of computed tomography and Nodule-Based risk models for detection of lung Cancer. J Thorac Oncol. 2017;12(3):578–84. https://doi.org/10.1016/j.jtho.2016.08.143.
15. Sullivan FM, Farmer E, Mair FS, et al. Detection in blood of autoantibodies to tumour antigens as a case-finding method in lung cancer using the EarlyCDT®-Lung test (ECLS): study protocol for a randomized controlled trial. BMC Cancer. 2017;17(1):187. https://doi.org/10.1186/s12885-017-3175-y.
16. Jiang D, Wang Y, Liu M, et al. A panel of autoantibodies against tumor-associated antigens in the early immunodiagnosis of lung cancer. Immunobiology. 2020;225(1):151848. https://doi.org/10.1016/j.imbio.2019.09.007.
17. Li N, Holden VK, Deepak J, Todd NW, Jiang F. Autoantibodies against tumor-associated antigens in sputum as biomarkers for lung cancer. Transl Oncol. 2021;14(2):100991. https://doi.org/10.1016/j.tranon.2020.100991.
18. Ouyang R, Wu S, Zhang B, et al. Clinical value of tumor-associated antigens and autoantibody panel combination detection in the early diagnostic of lung cancer. Cancer Biomark. 2021;32(3):401–9. https://doi.org/10.3233/CBM-210099.
19. Xu Y, Zhang W, Xia T, et al. Diagnostic value of tumor-associated autoantibodies panel in combination with traditional tumor markers for lung cancer. Front Oncol. 2023;13:1022331. https://doi.org/10.3389/fonc.2023.1022331.
20. Tang ZM, Ling ZG, Wang CM, Wu YB, Kong JL. Serum tumor-associated autoantibodies as diagnostic biomarkers for lung cancer: A systematic review and meta-analysis. PLoS One. 2017;12(7):e0182117. https://doi.org/10.1371/journal.pone.0182117.
21. American College of Radiology. Lung CT Screening Reporting and Data System (Lung-RADS™). 2019. Available from: https://www.acr.org/Clinical-Resources/Clinical-Tools-and-Reference/Reporting-and-Data-Systems/Lung-RADS.
22. Ren S, Zhang S, Jiang T, et al. Early detection of lung cancer by using an autoantibody panel in Chinese population. Oncoimmunology. 2017;7(2):e1384108. https://doi.org/10.1080/2162402X.2017.1384108.
23. Ding J, Li A, Hu Z, Wang L. Accurate pulmonary nodule detection in computed tomography images using deep convolutional neural networks. International conference on Medical Image Computing and Computer-Assisted Intervention. Springer, Cham, 2017, pp. 559–567.
24. Ren S, He K, Girshick R, Sun J, Faster R-CNN. Towards Real-Time object detection with region proposal networks. IEEE Trans Pattern Anal Mach Intell. 2017;39(6):1137–49. https://doi.org/10.1109/TPAMI.2016.2577031.
25. Detterbeck FC, Boffa DJ, Kim AW, Tanoue LT. The eighth edition lung Cancer stage classification. Chest. 2017;151(1):193–203. https://doi.org/10.1016/j.chest.2016.10.010.
26. González Maldonado S, Johnson T, Motsch E, Delorme S, Kaaks R. Can autoantibody tests enhance lung cancer screening?-an evaluation of EarlyCDT®-Lung in context of the German lung Cancer screening intervention trial (LUSI). Transl Lung Cancer Res. 2021;10(1):233–42. https://doi.org/10.21037/tlcr-20-727.
27. Chen P, Lu W, Chen T. Seven tumor-associated autoantibodies as a serum biomarker for primary screening of early-stage non-small cell lung cancer. J Clin Lab Anal. 2021;35(11):e24020. https://doi.org/10.1002/jcla.24020.
28. He YT, Zhang YC, Shi GF, Wang Q, Xu Q, Liang D, Du Y, Li DJ, Jin J, Shan BE. Risk factors for pulmonary nodules in North china: A prospective cohort study. Lung Cancer. 2018;120:122–9. https://doi.org/10.1016/j.lungcan.2018.03.021.
29. Meng Qingcheng G, Pengrui G, Lanwei, et al. Application of computer aided diagnosis system based on multi-stage 3D deep convolutional neural network in lung cancer screening. Chin J Radiol. 2020;54(6):552–6. https://doi.org/10.3760/cma.j.cn112149-20200414-00554-1.
30. Leidinger P, Keller A, Heisel S, et al. Novel autoantigens Immunogenic in COPD patients. Respir Res. 2009;10(1):20. https://doi.org/10.1186/1465-9921-10-20.
31. Schwartz-Albiez R, Monteiro RC, Rodriguez M, Binder CJ, Shoenfeld Y. Natural antibodies, intravenous Immunoglobulin and their role in autoimmunity, cancer and inflammation. Clin Exp Immunol. 2009;158(Suppl 1):43–50. https://doi.org/10.1111/j.1365-2249.2009.04026.x.

Publisher's note